PROSPECT-D: towards modeling leaf optical properties through a complete lifecycle

Jean-Baptiste Féret, A.A. Gitelson, S.D. Noble, S. Jacquemoud

in : Remote Sensing of Environment, vol. 193, n° may 2017, p.204-215

PROSPECT-D: towards modeling leaf optical properties through a complete lifecycle

J.-B. Féret[1], A.A. Gitelson[2, 3], S.D. Noble[4], S. Jacquemoud[5]

[1]Irtsea, UMR TETIS, Maison de la Télédétection, 500 Rue Jean François Breton, 34000 Montpellier, France

[2]Faculty of Civil and Environmental Engineering, Israel Institute of Technology, Technion City, Haifa, Israel

[3]School of Natural Resources, University of Nebraska, Lincoln, USA

[4]College of Engineering, University of Saskatchewan, 57 Campus Drive, Saskatoon, SK, S7N 5A9, Canada

[5]Institut de physique du globe de Paris - Sorbonne Paris Cité, Université Paris Diderot, UMR CNRS 7154, Case 7071, 35 rue Hélène Brion, 75013 Paris, France

Date: Friday, January 13, 2017

Keywords: Anthocyanins, Pigments, Hyperspectral, Leaf optical properties, PROSPECT, Radiative transfer model

Abstract

Leaf pigments provide valuable information about plant physiology. High resolution monitoring of their dynamics will give access to better understanding of processes occurring at different scales, and will be particularly important for ecologists, farmers, and decision makers to assess the influence of climate change on plant functions, and the adaptation of forest, crop, and other plant canopies. In this article, we present a new version of the widely-used PROSPECT model, hereafter named PROSPECT-D for dynamic, which adds anthocyanins to chlorophylls and carotenoids, the two plant pigments in the current version. We describe the evolution and improvements of PROSPECT-D compared to the previous versions, and perform a validation on various experimental datasets. Our results show that PROSPECT-D outperforms all the previous versions. Model prediction uncertainty is decreased and photosynthetic pigments are better retrieved. This is particularly the case for leaf carotenoids, the estimation of which is particularly challenging. PROSPECT-D is also able to simulate realistic leaf optical properties with minimal error in the visible domain, and similar performances to other versions in the near infrared and shortwave infrared domains.

1. Introduction

Climate change is expected to affect vegetation worldwide, influencing air temperature, biogeochemical cycles, and the frequency and intensity of plant disease. Leaf pigments are key components of life on Earth: they are major contributors to individual plant health via complex mechanisms allowing photosynthesis, plant growth, protection, adaptation to environmental changes and phenological events. Their dynamics directly affects nutrient, nitrogen, carbon and water cycles (Shipley et al., 2006; Joiner et al., 2011). Leaf pigments are therefore good indicators of changes in environmental conditions from local to global scales.

Three main families of pigments are found in leaves: chlorophylls, carotenoids, and anthocyanins. Chlorophyll–*a* and –*b*, the two types of molecules in higher plants, are the fundamental light-absorbing pigments involved in photosynthesis. Carotenoids are accessory pigments that contribute to light-harvesting and they also have essential photo-protective properties. If xanthophylls and carotenes are the two major divisions of the carotenoid group, more than 700 naturally occurring molecules have been identified so far, mainly in tissues other than leaves (Britton et al., 2004). Anthocyanins are part of the flavonoid family: they are closely associated with the colors in the autumn foliage of deciduous plant species. The term anthocyanin (*anthos* being Greek for flower, and *kyanos* for blue) has been used since Marquart (1835) to represent the coloring matter responsible for the various colors found in flowers, fruits and foliage in many plant species. The exception are the core Caryophyllales, most of which produce betalains (betacyanins and betaxanthins) (Brockington et al., 2011). While these betalain-producing families do include several species of notable agronomic interest, both crops and weeds, they represent a small fraction of plants investigated in a remote sensing context and are not considered in this work.

The anthocyanins include over 500 molecules, which accumulate in the vacuoles of various cells and tissues. They create a pink, red, purple or blue coloration in the tissue depending on the molecule, temperature, pH, and the presence or not of other molecules that may interact with them (Davies, 2004; Gould et al., 2009). Their role is still not fully understood and described. For example,

until recently their biosynthesis during senescence was suspected to be nature's extravagancy without a vital function, resulting from evolution in the absence of selection (Matile, 2000), and the reason for their presence was explained as a by-product of the flavonoid biosynthetic pathway. However, research over the past twenty years has demonstrated multiple functional implications of these pigments during the plant life cycle, to the point that they have been called the "Nature's Swiss army knife" by Gould (2004). Among the identified functions of anthocyanins are the protection of the photosynthetic apparatus from damage due to excess light (Lee and Gould, 2002), environmental stresses such as freezing or air pollution, plant pathogens, and predation (Lev-Yadun and Gould, 2008). An exhaustive review of the role of anthocyanins in plant leaves can be found in (Davies, 2004) and (Gould, 2004).

Leaf pigments interact with solar radiation and change in response to environmental conditions to optimize plant metabolism following complex pathways, within constraints of available resources and stressors. As a result, leaf optical properties are directly impacted by the composition of pigments. Remote sensing has proved to be a particularly suitable tool for the estimation of leaf pigments, both at level of the leaf (e.g., Féret et al., 2008; Gitelson et al., 2006; le Maire et al., 2004; Richardson et al., 2002; Sims and Gamon, 2002) and the canopy (e.g., Asner et al., 2015b; Atzberger et al., 2010; Gitelson et al., 2005; Haboudane, 2004; Hmimina et al., 2015). The retrieval of pigment content from remote sensing data involves two main approaches. The first approach is data-driven. It includes univariate statistical models derived from spectral indices (e.g., Gitelson et al., 2006), multivariate statistical models such as partial least squared regressions (e.g., Asner and Martin, 2009) and machine learning algorithms (e.g., Verrelst et al., 2015). The relationships derived from these predictive models are usually established empirically; they strongly depend on the variability and quality of the data used to adjust these models, therefore they may lack robustness. The second approach is based on radiative transfer models that exist both at leaf and canopy scales. Leaf models generally simulate their spectral directional-hemispherical reflectance and transmittance while canopy models simulate their spectral and bidirectional reflectance assuming that the leaf and soil

optical properties, the vegetation architecture, and the conditions of acquisition are known. The combination of the two approaches (data-driven and physical) is also becoming increasingly popular because it provides alternatives to extensive data collection required by the first, and high computational resources required by the second (Féret et al., 2011; Verrelst et al., 2015).

To date, most studies devoted to vegetation pigments have focused on chlorophyll. This can be explained by multiple factors. First, leaf chlorophyll content is the variable that has the strongest effect on canopy reflectance in the VIS, and is a valuable proxy of nitrogen content and gross primary production (e.g., Gitelson et al., 2012; Peng and Gitelson, 2012), which have strong impact in terms of food and biomass production globally. Second, leaf chlorophyll content can be estimated with relatively good accuracy using simple statistical regression models based on the relationship between this variable and various spectral indices (e.g. Féret et al., 2011; Gitelson et al., 2006; le Maire et al., 2004). Third, the availability of physical models including chlorophyll as input parameters allowed investigating and better understanding its influence on the signal measured by satellite sensors, leading to improved predictive models for leaf and canopy chlorophyll content in a more systematic way than experimental data collection would have permitted. This is the case of the combined PROSPECT leaf optical properties model (Jacquemoud and Baret, 1990) and SAIL canopy bidirectional reflectance model (Verhoef, 1984; Verhoef et al., 2007), also referred to as PROSAIL, which has been used for more than 25 years (Jacquemoud et al., 2009).

Current challenges such as food security, global warming and massive biodiversity loss now require fine monitoring of vegetation status, with a level of information beyond inputs provided by chlorophyll content alone. We need to address various issues related to vegetation, including stress, invasive species, plant diseases and photosynthetic phenology, which implies monitoring the dynamic of various pigment types such as carotenoids (Gamon et al., 2016) and anthocyanins. One of the most studied “pigment-related” indicators derived from remote sensing is the Photochemical Reflectance Index (PRI, Gamon et al., 1992) based on two narrow spectral bands in the green spectrum: the PRI related to the xanthophyll cycle in the leaf; it captures the physiological response

of vegetation in response to a short term environmental stress inducting slight changes in photosynthetic activity (Gamon et al., 1997, 1992, 1990). However, the primary driver of the PRI over long time periods, at both leaf and canopy scales, is not the xanthophyll cycle, but rather the changing leaf carotenoid pigment pool, typically expressed as the changing ratio of chlorophyll to carotenoid pigments (or its inverse) (Filella et al., 2009; Nakaji et al., 2006; Stylinski et al., 2002). Therefore, information about pigment content in vegetation is crucial when monitoring photosynthetic phenology. At local scale, estimating pigment content from individuals using portable devices, close range remote sensing or UAV can be useful for monitoring purposes in precision agriculture or ecophysiology. At global scale, the ability to precisely monitor photosynthetic phenology with satellite imagery is extremely valuable and would provide important input for models of global terrestrial carbon uptake. Few studies focus on the direct estimation of carotenoids at leaf scale (Chappelle et al., 1992; Gitelson et al., 2006, 2001; Sims and Gamon, 2002) and canopy scale (Asner et al., 2015a, 2015b; Gamon et al., 2016; Hernández-Clemente et al., 2014, 2012; Ustin et al., 2009; Zarco-Tejada et al., 2013). Even fewer focus on the estimation of anthocyanin, also at leaf (Gamon and Surfus, 1999; Gitelson et al., 2001, 2006; Sims and Gamon, 2002; Steele et al., 2009) and canopy (Rundquist et al., 2014) scales. The presence of overlapping features in the specific absorption coefficient (SAC) of carotenoids and anthocyanins makes it difficult to separate and quantify these accessory pigments using basic methods such as spectral indices, especially at canopy scale (Ustin et al., 2009).

Monitoring vegetation status, stress, and shifts in the ecosystem functional properties is critical. It will require sophisticated methods of leaf pigment content estimation, possibly combined with the next generation of high resolution imaging spectrometers like Hyspiri (NASA), EnMAP (DLR) or Hypxim (CNES), and vegetation radiative transfer models that incorporate all major pigments. Present leaf optical properties models do not include pigments other than chlorophylls and carotenoids, limiting the application of the physical approach to the study of these pigments (Blackburn, 2007). SLOP (Maier et al., 1999), PROSPECT-5 (Féret et al., 2008), and soon after LIBERTY,

specifically designed for pine needles (Di Vittorio, 2009), are the three models that use carotenoids. The dorsiventral leaf model designed by Stuckens et al. (2009) also differentiates chlorophylls from carotenoids, but the SACs are those used in PROSPECT-5.

This article introduces a new version of the widely-used PROSPECT model, called PROSPECT-D, which for the first time includes all three main pigments that control the optical properties of fresh leaves, i.e., chlorophylls, carotenoids, and anthocyanins. The suffix -D stands for "dynamic" because the model makes it possible to simulate leaf optical properties through a complete lifecycle, from emergence, to anthocyanin-expressing stress responses, through to senescence. Given the success and widespread use of PROSPECT-5, a major requirement for the development of PROSPECT-D was to preserve, and ideally to improve on, the performance of PROSPECT-5 for pigment estimation in samples containing little or no anthocyanin, while adding support for those that do. We performed a new calibration of the SAC of each pigment, and updated the refractive index used by the model. PROSPECT-D was then tested on several datasets displaying many plant species with a large range of leaf traits including pigment composition. We evaluated its performance using two criteria resulting from iterative optimization of leaf chemical and structural properties: the difference between the measured and the modeled leaf directional-hemispherical reflectance and transmittance spectra, and the accuracy of corresponding pigment estimation. We compared these two criteria for the new and current versions of the model.

2. Calibration of the model

Several strategies for the calibration of PROSPECT have been investigated since its first version. All of the procedures have points in common, such as the adjustment of one or several optical constants (SAC of leaf chemical constituents, refractive index) over the VIS, near infrared and shortwave infrared (SWIR) domains. A standard method consists in determining the optical constants individually or simultaneously at each wavelength by using an iterative procedure (Féret et al., 2008; Li and Wang, 2011). So far, there is no unique method, and adaptations have been proposed to

159 calibrate PROSPECT: Malenovský et al. (2006) adjusted SACs for needle-shaped leaves; Féret et al.
160 (2008) have simultaneously determined the refractive index and SAC of leaf constituents; Chen and
161 Weng (2012) have computed an individual refractive index for each leaf sample. In this section, we
162 provide information about the calibration of PROSPECT-D, including the selection of the calibration
163 dataset, as well as the main steps leading to updated optical constants.

164 **2.1. Available datasets**

165 Six independent datasets collected by several researchers for diverse purposes have been used
166 in this study (Table 1). They share directional-hemispherical reflectance and/or transmittance
167 spectra, and at least two pigments out of three (chlorophylls, carotenoids, and anthocyanins)
168 measured using wet chemistry. The ANGERS dataset includes more than 40 plant species; all the
169 other datasets are monospecies: European hazel (*Corylus avellana* L.) in HAZEL, Norway maple (*Acer*
170 *platanoides* L.) in MAPLE, Virginia creeper (*Parthenocissus quinquefolia* (L.) Planch) in VIRGINIA, and
171 Siberian dogwood (*Cornus alba* L.) in DOGWOOD-1 and -2. Table 1 summarizes the spectral and
172 chemical information available for each dataset. Additional information about the protocols used to
173 conduct the experiments, collect the leaves, measure their optical properties and determine their
174 wet chemistry can be found in (Féret et al., 2008; Gitelson et al., 2009, 2006, 2001; Merzlyak et al.,
175 2008). Note that DOGWOOD-2 does not contain transmittance spectra; that the total chlorophyll
176 content (C_{ab}, expressed in µg cm^{-2}) is available in all datasets; that the total carotenoid content (C_{xc},
177 expressed in µg cm^{-2}) and the total anthocyanin content (C_{anth}, expressed in µg cm^{-2}) have not been
178 determined in HAZEL and ANGERS, respectively. Finally, the 400-780 nm spectral range used for the
179 calibration of the pigment content is common to all datasets except DOGWOOD-1.
180

Table 1. Description of the leaf datasets used in this study. * The ANGER dataset is available online http://opticleaf.ipgp.fr/index.php?page=database.

Database	Reference	Spectral range (nm)	Number of leaves	Optical properties	Chlorophyll content C_{ab} (µg cm^{-2})			Carotenoid content C_{xc} (µg cm^{-2})			Anthocyanin content C_{anth} (µg cm^{-2})		
					Mean ± SD	Min	Max	Mean ± SD	Min	Max	Mean ± SD	Min	Max
ANGERS*	1, 2	400-2500	308	R & T	34.41 ± 21.85	0.78	106.70	8.84 ± 5.14	0.00	25.28	N/A	N/A	N/A
VIRGINIA	3, 4	400-800	81	R & T	11.05 ± 14.60	0.09	53.76	2.98 ± 3.06	0.15	12.27	8.63 ± 10.77	0.00	37.50
MAPLE	3, 4, 6	400-780	48	R & T	7.43 ± 7.36	0.14	32.98	5.25 ± 2.37	1.82	10.40	8.75 ± 6.83	1.12	21.66
DOGWOOD-1	3, 4, 5	440-796	20	R & T	4.53 ± 4.84	0.07	15.03	2.96 ± 2.06	0.42	5.71	6.88 ± 5.52	0.40	15.49
HAZEL	3, 4	400-800	13	R & T	26.37 ± 3.55	22.69	34.62	N/A	N/A	N/A	7.13 ± 4.19	0.25	13.61
DOGWOOD-2	6	400-1000	51	R	23.77 ± 7.58	1.53	39.81	5.39 ± 2.26	1.73	10.76	12.71 ± 8.21	1.07	30.23

1: Féret et al. (2008); 2: Féret et al. (2011); 3: Merzlyak et al. (2008); 4: Gitelson et al. (2009); 5: Gitelson et al., (2001); 6: Gitelson et al. (2006).

184

185 **2.2. Data selection for calibration**

186 The calibration of PROSPECT-D requires the leaf samples to have general properties at a
187 minimal level: *i)* pigment content expressed in the same unit for chlorophylls, carotenoids, and
188 anthocyanins, and *ii)* reflectance and transmittance spectra in the 400-780 nm wavelength range. A
189 challenge to calibrating a high performance leaf optical properties model is the lack of
190 comprehensive datasets meeting these two criteria. Among those available, only VIRGINIA and
191 MAPLE fulfill these conditions. Preliminary calibration tests using part or all of these datasets led to
192 SACs with strong discrepancies and poor performances for the estimation of pigment content.
193 Therefore we considered alternative methods combining different data sources and expanding the
194 pool of available calibration data to fill in the gaps. Féret et al. (2008) exploited the ANGERS dataset
195 to calibrate PROSPECT-4 and -5. It is characterized by a wide range of leaf types and pigment
196 contents, and it proved to be well suited for the determination of the SAC of the chlorophyll and
197 carotenoid pigments. These desirable properties of ANGERS come from the variety of leaf types:
198 while chlorophyll and carotenoids contents are usually highly correlated in mature leaves, ANGERS
199 includes juvenile, stressed and senescent leaves lowering this correlation and allowing the SAC of
200 each of these pigments to be adjusted independently from the others, despite their overlapping
201 domain of absorption. Therefore we took the decision to include ANGERS in the calibration dataset
202 and to estimate the corresponding C_{anth} using a spectral index. To avoid the associated uncertainty
203 leading to errors in the SACs, we combined a subset of ANGERS with a subset of VIRGINIA that
204 included accurate measurements of C_{anth} obtained by wet chemistry (Merzlyak et al., 2008). Leaves
205 from VIRGINIA were collected in a park at Moscow State University; they contained very high levels
206 of anthocyanin and low to moderate levels of chlorophyll and carotenoids; they displayed the
207 maximum range of anthocyanin among all the available datasets. In this section, we first explain how
208 C_{anth} was estimated in ANGERS, and then how we split ANGERS and VIRGINIA into calibration and

validation subsets. Finally, we present a sensitivity study intended to analyze the influence of the expected C_{anth} uncertainty in ANGERS on the performances of the model.

2.2.a. Estimation of leaf anthocyanin content in ANGERS

Several nondestructive methods to estimate C_{anth} from leaf reflectance have been identified and tested on experimental data for which the anthocyanin content has been measured. These methods included spectral indices and machine learning algorithms such as support vector regression (Gitelson et al., 2001, 2006, 2009; van den Berg and Perkins, 2005; Pfündel et al., 2007). The modified Anthocyanin Reflectance Index ($mARI$) designed by Gitelson et al. (2006) led to the best results when using a leave-one-out cross-validation. This index is defined by:

$$mARI = \left(R_{green}^{-1} - R_{red\ edge}^{-1}\right) \times R_{NIR} \qquad \text{Eq. 1}$$

where R_{green} is the mean reflectance between 540 nm and 560 nm, $R_{red\ edge}$ the mean reflectance between 690 nm and 710 nm, and R_{NIR} the mean reflectance between 760 nm and 800 nm. We first studied the relationship between $mARI$ and C_{anth} over the 213 samples for which information about anthocyanins was available, i.e., all datasets of Table 1 with the exception of ANGERS. We found a strong linear relationship for $mARI$ values smaller than 5 (137 samples, R^2 = 0.90, RMSE = 1.18 µg cm^{-2}) and a weak one for $mARI$ values greater than 5 (76 samples, R^2 = 0.37, RMSE = 6.35 µg cm^{-2}) (Figure 1). These samples with $mARI < 5$ correspond to mature green, yellow, and reddish/red leaves with C_{anth} values less than 12 µg cm^{-2}. Leaves with C_{anth} values higher than 12 µg cm^{-2} are generally dark red and contain small amounts of chlorophyll. In that case, absorptance between 540 nm and 560 nm exceeded 90% and further increases of anthocyanin did not change leaf optical properties. A linear model for anthocyanin estimation (Eq. 2) was then derived from the subset excluding the samples with $mARI > 5$ and $C_{anth} > 12\ \mu g\ \mathrm{cm}^{-2}$.

234

$$C_{anth} = 2.11 \times mARI + 0.45 \quad \text{Eq. 2}$$

235

236 Eq. 2 was applied to the ANGERS dataset to determine C_{anth}. The anthocyanin content ranged

237 from 0 to 17.1 µg cm^{-2}, with a mean value of 1.7 µg cm^{-2}.

238

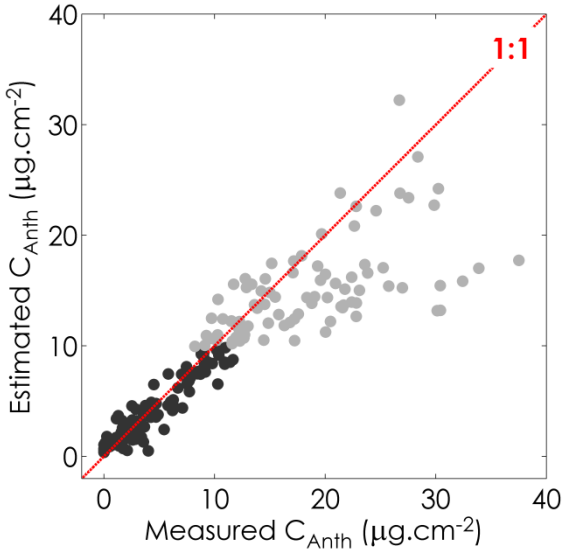

Figure 1. Relationship between C_{anth} obtained from wet chemistry and C_{anth} estimated from reflectance data after application of Eq. 2. The black dots correspond to the 137 leaf samples with $mARI < 5$ (R^2 = 0.90) and the grey dots correspond to the 76 leaf samples with $mARI > 5$ (R^2 = 0.37). Eq. 2 was adjusted only on the black dots.

239 ***2.2.b. Selection of the calibration samples***

240 In order to keep as many samples as possible, we decided to build a calibration dataset made of leaf

241 samples selected both in ANGERS and VIRGINIA. The influence of the uncertainty associated to C_{anth}

242 in ANGERS is expected to be mitigated by the accuracy of C_{anth} in VIRGINIA.

243 In VIRGINIA we identified samples characterized by low C_{ab} ($< 20\ \mu g\ cm^{-2}$) and C_{xc} ($< 5\ \mu g\ cm^{-2}$)

244 in order to decrease the combined influence of the pigments on leaf optical properties, but also to

245 minimize the correlation among pigments. It should allow capturing the influence of anthocyanins

independently from the other pigments. We randomly selected 20 samples, leaving a total of 61 samples of VIRGINIA for the validation.

In ANGERS we discarded at first 14 atypical samples, the spectral behavior of which was incompatible with PROSPECT assumptions. For example, we removed samples collected on *Eucalyptus gunnii* and *Cornus alba*, the overall reflectance of which was very high in the VIS because of the presence of wax (Barry and Newnham, 2012); and three samples of *Schefflera arboricola* displaying uncharacteristic optical properties in the blue (400-450 nm). We also removed samples with $mARI > 5$ as the uncertainty associated to C_{anth} was particularly high (Figure 1). Finally we eliminated leaf samples that had little influence on the calibrated SACs. For that purpose we determined a reference SAC for each pigment using the 314 preselected leaf samples (20 from VIRGINIA and 294 from ANGERS). The ANGERS samples inducing changes in the SACs higher than 5% between 425 nm and 475 nm were kept in the calibration datasets, the others were transferred to the validation dataset.

In total, a dataset named CALIBRATION and combining subsets of ANGERS (144 samples) and VIRGINIA (20 samples) was used for the calibration phase.

2.2.c. Sensitivity of the calibration to the uncertainty associated with C_{anth} in ANGERS

As abovementioned, determining C_{anth} with a spectral index like $mARI$ leads to uncertainty likely to impact the quality of the calibration. We performed a sensitivity analysis with the aim of understanding the influence of this uncertainty on the SACs and on the overall performances of the model. It consisted in adding a Gaussian noise (σ = 1.18 µg cm^{-}2) to C_{anth} in ANGERS prior to the calibration and validation procedure. We repeated the operation 50 times.

2.3. Selection of the refractive index

PROSPECT is based on the generalized plate model proposed by (Allen et al., 1970, 1969). A plant leaf is modeled as a pile of elementary layers characterized by an absorption coefficient and a refractive index provided at a given wavelength. In the first version of the model, Jacquemoud and

Baret (1990) used an albino maize leaf to obtain an experimental spectrum of the refractive index for the elementary layers. le Maire et al. (2004) and Féret et al. (2008) adopted a new strategy based on numerical optimization to determine the optical constants of PROSPECT at the same time. Their refractive index performed slightly better than the previous versions at estimating leaf chemical constituents, but the strong spectral variations observed in the visible wavelengths induced small artifacts in the optical properties of leaves displaying high pigment content. Stuckens et al. (2009) also adjusted a unique refractive index for all leaves.

Attempts to obtain a unique refractive index spectrum for all leaves are actually unfounded and inconsistent with the Kramers-Kronig relations that state that the real (refractive index) and imaginary (absorption coefficient) parts of the complex refractive index of a medium are physically linked (Lucarini et al., 2005). These relations allow direct computation of the refractive index of a medium based on its absorption properties on an extended spectral domain. Chen and Weng (2012) used the Kramers-Kronig relations to derive an effective refractive index adjusted to each leaf sample, obtaining very promising results. However, leaf chemical and spectral databases are often incomplete; in particular they cover a limited range of the electromagnetic spectrum, so such a method is impracticable. As a consequence we considered the refractive index to be independent of the leaf sample in this study, but changed strategy compared to PROSPECT-5 in order to avoid the abovementioned artifacts resulting from numerical optimization. Two options were tested: 1) using the refractive index imbedded in PROSPECT-3, and 2) taking the average refractive index derived from minimum and maximum values computed by Chen and Weng (2012) and corresponding to the boundaries of the grey area in Figure 2. The spectra displayed in Figure 2 strongly differ in shape in the VIS: the overall profile of the refractive indices computed by Chen and Weng (2012) is quite similar to that measured for pure liquid water (Hale and Querry, 1973), gradually decreasing from the visible to the infrared, whereas the indices in PROSPECT-3 and -5 are very much alike in the near and shortwave infrared (1000-2500 nm) and show a steeper decrease. Divergence between the refractive index derived from Chen and Weng (2012) and those used in PROSPECT-3 and -5 strongly increases

298 with wavelength. We performed the full calibration of PROSPECT (including optimal adjustment of
299 SAC as described in Section 2.2.b) with each refractive index.
300

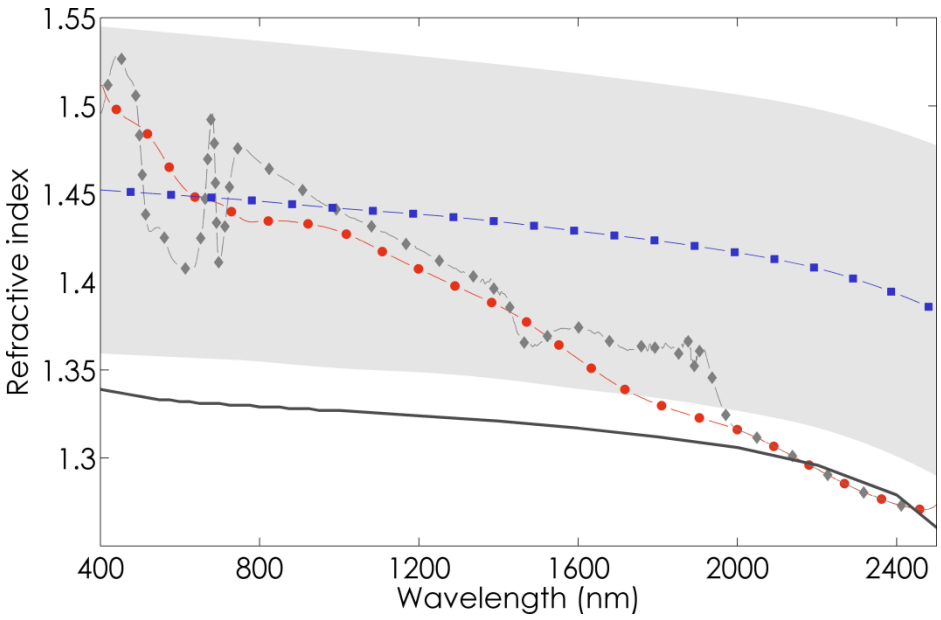

Figure 2. Comparison of the refractive index used in PROSPECT-3 (red dots), PROSPECT-5 (grey diamonds) and corresponding to the mean refractive index proposed by (Chen and Weng, 2012) (blue squares). The grey area corresponds to the range of variation of the refractive index proposed by Chen and Weng, (2012); the plain grey line corresponds to the refractive index for pure liquid water (Hale and Querry, 1973).

301

302 **2.4. Optimal adjustment of the specific absorption coefficients**

303 The adjustment of the SAC for each group of pigments is based on numerical optimization
304 routines applied to experimental data. As in PROSPECT-5 we assumed that the chlorophyll *a*:*b* ratio
305 was constant and we combined carotenes and xanthophylls in the carotenoid group. Similarly
306 anthocyanins were assumed to include all types of anthocyanins contributing to light absorption in
307 the VIS. Given the well-known sensitivity of the anthocyanin absorption properties to pH, which is
308 due to a reversible structural change that occurs in the C ring of the molecule, this hypothesis may be

incorrect in certain situations. However, environment inside a vacuole is generally slightly acid, with pH values reported to fall within the range of 5.0 to 6.0 pH units, with a mean pH of 5.5 (Mathieu et al., 1989; Martinière et al., 2013).

Solved SAC values were constrained to be positive. To prevent erroneous absorption assignments, the wavelength domains were narrowed to 400-750 nm for chlorophylls, 400-560 nm for carotenoids, and 400-660 nm for anthocyanins. These ranges are broader than *in vitro* due to the detour effect: the lengthening of the optical path-length within the leaf results in substantial flattening of the absorption spectrum *in vivo* (e.g., Rühle and Wild, 1979; Fukshansky et al., 1993).

The calibration followed a two-steps algorithm described in Féret et al. (2008). First, we determined the structure parameter N_j of each leaf j in the calibration datasets on the basis of an iterative optimization: N_j was estimated based on a multivariate iterative optimization, simultaneously with three absorption coefficients using reflectance and transmittance values measured at three wavelengths corresponding to the minimum absorptance (λ_1), maximum reflectance (λ_2), and maximum transmittance (λ_3) of the leaf. These values are generally located on the NIR plateau. The iterative optimization was performed using the merit function:

$$M_{leafN}\left(N_j, k(\lambda_1), k(\lambda_2), k(\lambda_3)\right) = \sum_{l=1}^{3}\left(R_{meas,j}(\lambda_l) - R_{mod}\left(N_j, k(\lambda_l)\right)\right)^2 + \left(T_{meas,j}(\lambda_l) - T_{mod}\left(N_j, k(\lambda_l)\right)\right)^2 \quad \text{Eq. 3}$$

with $R_{meas,j}(\lambda_l)$ and $T_{meas,j}(\lambda_l)$ the measured reflectance and transmittance of leaf j at the wavelength λ_l, R_{mod} and T_{mod} the modeled values, and $k(\lambda)$ the absorption coefficient of a compact layer at the wavelength λ, which is adjusted simultaneously with N_j. In Eq. 3, $k(\lambda)$ is not decomposed into specific absorption of the different chemical constituents. This step occurs in the NIR where pigments have little if any influence, so $k(\lambda)$ is primarily affected by water absorption.

The SAC to be calibrated were then computed by inverting PROSPECT on the $n = 164$ leaves of the calibration dataset. We minimized the merit function J at each wavelength:

$$J\left(\{K_{spe,i}(\lambda)\}_{i=1:n}\right) = \sum_{j=1}^{n}\left(R_{meas,j}(\lambda) - R_{mod,j}\left(N_j, k(\lambda)\right)\right)^2 + \left(T_{meas,j}(\lambda) - T_{mod,j}\left(N_j, k(\lambda)\right)\right)^2 \quad \text{Eq. 4}$$

where

$$k(\lambda) = \frac{\sum_i K_{spe,i}(\lambda) \times C_{i,j}}{N_j} \quad \text{Eq. 5}$$

$k(\lambda)$ is the absorption coefficient of a compact layer at the wavelength λ, $K_{spe,i}(\lambda)$ is the SAC of constituent i, $C_{i,j}$ is the corresponding content for leaf j, N_j is the leaf structure parameter of leaf j, and n corresponds to the number of biochemical constituents for which the SACs are simultaneously calibrated.

3. Validation: datasets and criteria for the comparison of model performances

We performed model inversions on the validation dataset with PROSPECT-D, as well as PROSPECT-3 and -5. The performances of the different versions of the model were compared in terms of pigment content estimation and leaf spectra fit. The validation was performed using all leaf samples after exclusion of the calibration samples.

PROSPECT was inverted on the validation dataset using an iterative method for optimization. It consists in finding the best combination of leaf chemical and structural parameters that minimizes the merit function:

$$M_{inv}\left(N,\{C_i\}_{i=1:p}\right) = \sum_{\lambda=1}^{n_\lambda}\left(R_{meas,\lambda} - R_{mod,\lambda}\left(N,\{C_i\}_{i=1:p}\right)\right)^2 + \left(T_{meas,\lambda} - T_{mod,\lambda}\left(N,\{C_i\}_{i=1:p}\right)\right)^2 \quad \text{Eq. 6}$$

with n_λ the number of available spectral bands, N the leaf structure parameter, C_i the content of constituent i, and p the number of leaf biochemical constituents. In this study, we simultaneously estimated the six input parameters of PROSPECT: pigments (C_{ab}, C_{xc}, C_{anth}), equivalent water thickness (EWT), leaf mass per area (LMA) and leaf structure parameter (N).

In essence, candidate sets of these parameters are iteratively input in forward mode and the resulting modeled reflectance and/or transmittance spectra compared against the measured ones; the parameter are revised until the minimum value of the merit function is found. When the assumptions of the model are not met, for example if a pigment is not taken into account, or if the SACs are incorrect, the inversion will converge towards a suboptimal solution, inducing errors in the estimation of the parameters. This situation occurs when we try to invert PROSPECT-3 on yellowing leaves; C_{ab} is overestimated to compensate for the absorption of C_{xc}.

The root mean square error (*RMSE* expressed in µg cm^{-2}) can be computed to appraise the difference between the measured and estimated pigment content:

$$RMSE = \sqrt{\frac{\sum_{j=1}^{n}\left(X_{meas,j} - X_{mod,j}\right)^2}{n}} \quad \text{Eq. 7}$$

where $X_{meas,j}$ are the measured values and $X_{mod,j}$ are the values estimated by model inversion for leaf j. As for the quality of the fit, it is appraised by the spectral RMSE which calculates the difference between the measured and simulated reflectance and transmittance spectra on a wavelength-by-wavelength basis.

4. Results

375 **4.1. Selection of a calibration dataset**

376 Figure 3 shows the pigment distribution corresponding to the calibration and validation
377 samples in ANGERS and VIRGINIA: note that the calibration samples display low to moderate C_{ab} and
378 C_{xc} values, whereas the validation samples encompasses significantly broader pigment contents. The
379 calibration samples with high C_{anth} come from VIRGINIA, for reasons explained earlier.

380

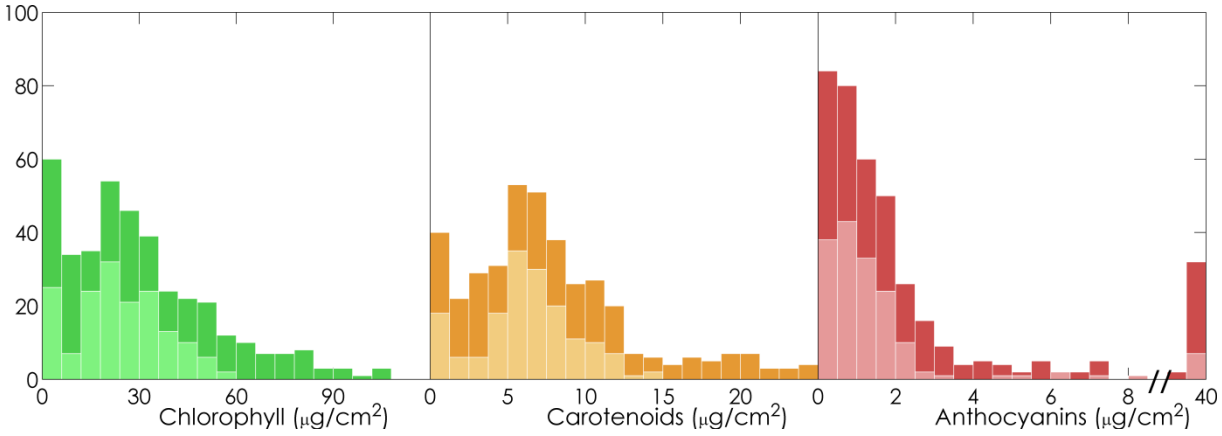

Figure 3. Stacked distribution of pigment content for the calibration and validation samples selected from ANGERS and VIRGINIA. Light colors: calibration (144 samples from ANGERS, 20 Samples from VIRGINIA); dark colors: validation (164 samples from ANGERS, 61 samples from VIRGINIA).

381

382 **4.2. Selection of the refractive index**

383 The refractive index spectra displayed in Figure 2 provide advantages and disadvantages in
384 terms of model accuracy both for the estimation of leaf chemistry and the simulation of leaf optical
385 properties. We performed calibrations of PROSPECT-D as detailed in Section 3, using either the
386 refractive index of PROSPECT-3 and the one derived by Chen and Weng (2012). Then we inverted the
387 two versions of the model on ANGERS, the only dataset covering the SWIR as well as including
388 measurements of EWT and LMA. Overall the performances obtained for pigment retrieval and
389 simulation of leaf optics were similar in the VIS. For water and dry matter, results were also very

similar. Simulated leaf reflectance and transmittance spectra also exhibited very slight differences in the VIS, while they were noticeable in the NIR and SWIR. This is illustrated by Figure 4 that displays the spectral RMSE calculated between measured and simulated leaf spectra for ANGERS. The reflectances are comparable, with slightly higher RMSE obtained with the refractive index derived from Chen and Weng (2012) between 1500 nm and 1900 nm; there are higher discrepancies in the transmittances. Based on these results, we assigned the refractive index used in PROSPECT-3 to PROSPECT-D.

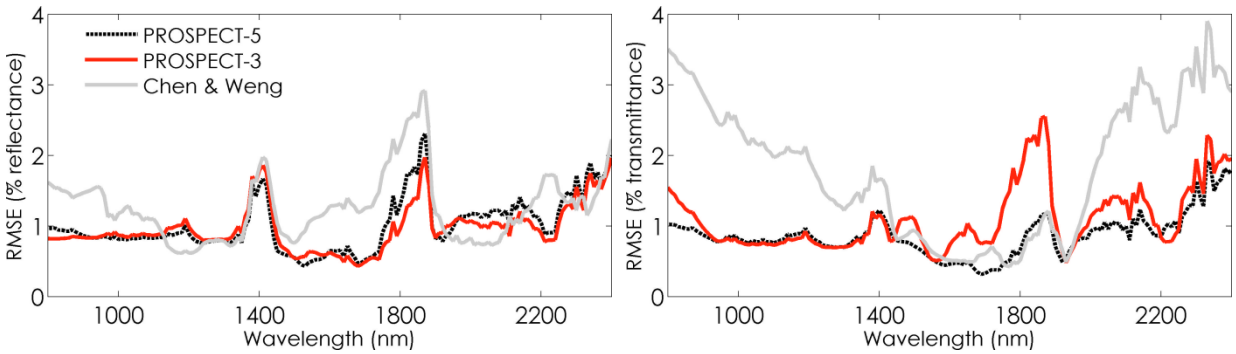

Figure 4. Spectral RMSE between measured leaf optics and simulated reflectance (left), and transmittance (right) obtained after model inversion with the refractive index used in PROSPECT-5 (black dotted line), PROSPECT-3 (red), and derived from Chen and Weng (2012) (light grey).

4.3. Adjustment of the specific absorption coefficients

Figure 5 displays the SACs of pigment in PROSPECT-5 and PROSPECT-D. The differences between the two models are minor for chlorophylls and carotenoids beyond 450 nm. However, noticeable differences can be observed for carotenoids between 400 nm and 450 nm: compared to PROSEPCT-D, the SAC of C_{xc} sharply increases towards the ultraviolet (UV) domain in PROSPECT-5, possibly due to the presence of flavonoids in the calibration samples. This augmentation is compensated by a slight decrease of the SACs of C_{ab} and C_{anth}. The SAC of anthocyanins shows a strong absorption between 450 nm and 650 nm, that peaks at about 550 nm. This result is in

agreement with the absorption spectra reported in the literature (Dougall and Baker, 2008; Peters and Noble, 2014). The broadness of the absorption peak may be caused by calibration artifacts related to residual correlations between the pigments.

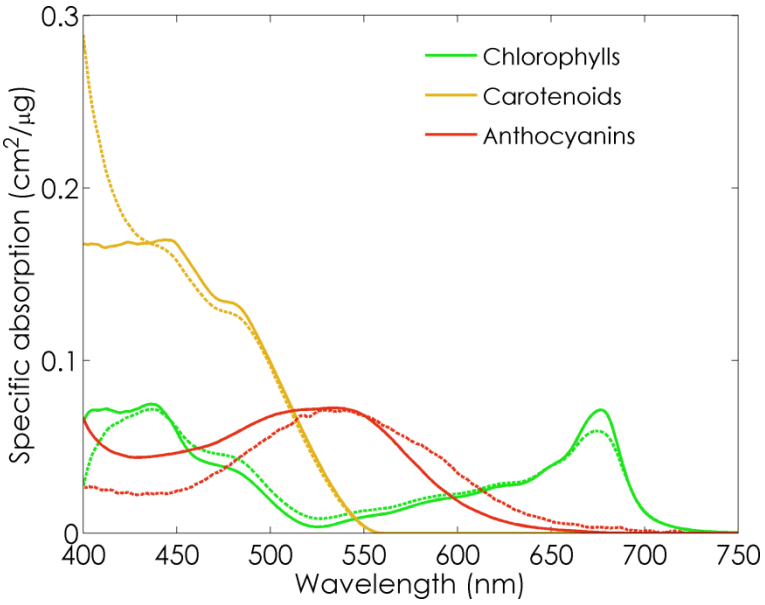

Figure 5. Specific absorption coefficients of chlorophylls (green), carotenoids (orange), and anthocyanins (red). The solids line correspond to the SAC of all the pigments in PROSPECT-D, the dashed lines to the SAC of chlorophylls and carotenoids in PROSPECT-5, and to the SAC of anthocyanins measured by Peters and Noble (2014) using thin layer chromatography.

4.4. Validation of model performances

4.4.a. Estimation of leaf pigment by PROSPECT inversion

C_{ab}, C_{xc} and C_{anth} have been estimated by inversion of PROSPECT-D on a dataset hereafter called VALIDATION. It gathered all experimental datasets (Table 1) except DOGWOOD-2 which did not contain transmittance spectra. ANGERS was also excluded for anthocyanins since C_{anth} has been indirectly estimated using a spectral index.

Table 2 compares the performances of PROSPECT-3, -5 and -D for pigment estimation in terms of RMSE. One can note a markedly improvement of C_{xc} estimation by PROSPECT-D for all datasets. In

ANGERS, which mainly contain green leaves, PROSPECT-5 and PROSPECT-D perform similarly at estimating C_{ab}, with a slight increase of RMSE obtained with PROSPECT-D. It can be explained by the fact that these samples correspond to calibration samples in PROSPECT-5. PROSPECT-D surpasses the previous versions of the model for all datasets other than ANGERS. Importantly, the new model is able to accurately estimate C_{xc} even in anthocyanic leaves, which has been problematic for other techniques.

Table 2. RMSE (µg cm^{-2}) of the estimation of leaf pigment content using PROSPECT-3 (P-3), PROSPECT-5 (P-5), and PROSPECT-D (P-D) inversion. The bold font for numbers indicates the lowest values.

Database	C_{ab}			C_{xc}		C_{anth}
	P-3	P-5	P-D	P-5	P-D	P-D
CALIBRATION	6.84	3.69	**3.43**	6.69	**1.31**	1.74
ANGERS (VAL)	11.07	**6.71**	7.07	6.90	**3.81**	3.22
MAPLE	15.54	7.85	**3.28**	17.28	**2.23**	2.34
VIRGINIA (VAL)	14.38	7.74	**2.95**	17.41	**1.19**	4.54
DOGWOOD-1	14.94	7.90	**3.12**	18.07	**1.21**	2.24
HAZEL	20.88	9.67	**2.36**	n.a.	**n.a.**	2.82
DOGWOOD-2	37.22	16.51	**6.08**	20.92	**10.92**	14.39
VALIDATION	13.33	7.33	**5.58**	12.67	**3.06**	3.49

Figure 6 illustrates the differences observed in Tables 2. PROSPECT-3 overestimated C_{ab} for all datasets, even with ANGERS which mainly contained green leaves; this overestimation was reduced when using PROSPECT-5 or PROSPECT-D. The substantial improvement in C_{xc} estimation when using PROSPECT-D is a significant result of this article: overall, the RMSE was divided by four compared to the results obtained with PROSPECT-5. The inversion of PROSPECT-5 on anthocyanin-rich leaves sometimes converged towards the upper bound on C_{xc} (30 µg cm^{-2}). It is likely that this overestimation of carotenoid content results from the strong absorption of light by anthocyanins in the same wavelength range as carotenoids, and this absorption is not properly modeled by PROSPECT-5. In ANGERS, the systematic underestimation of C_{xc} by PROSPECT-5 in leaves containing high amounts of photosynthetic pigments was greatly reduced by PROSPECT-D. The overestimation

441 of C_{xc} in anthocyanin-rich leaves was also corrected. The lower performances of PROSPECT-D on
442 DOGWOOD-2 are probably explained by the absence of transmittance spectra. As explained in
443 Section 4.1, the samples selected for the calibration dataset in ANGERS were marked out by low to
444 medium pigment content, therefore they were not representative of the full range of variation found
445 in this dataset: nevertheless, this did not prevent us from estimating high pigment content with
446 accuracy. This is explained by slight changes in the optical properties of leaves with high-pigment
447 content when carotenoids increase, due to saturation effects. It also suggests that the physical
448 description used in PROSPECT is correct, as its ability to estimate pigment content goes beyond the
449 range used for calibration. Samples showing underestimated C_{xc} in ANGERS were discarded from the
450 calibration dataset due to unusual optical properties (surface effects) or very high $mARI$.

451

452

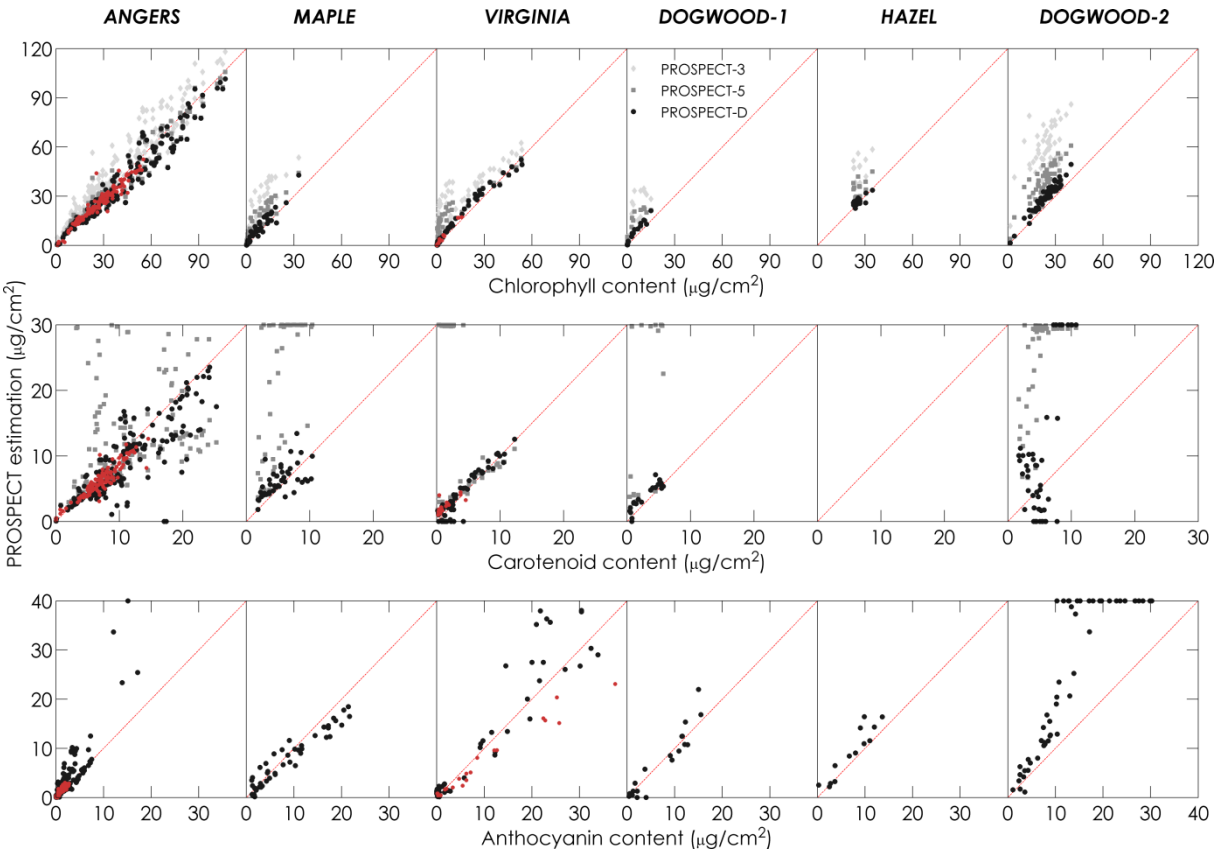

Figure 6. Estimation of pigment content by inversion of three versions of PROSPECT on six datasets

(when relevant). Red dots correspond to calibration samples from ANGERS and VIRGINIA.

453

454 4.4.b. Spectrum reconstruction

455 We compared the spectral RMSE between measured spectra and spectra reconstructed by the
456 last three versions of PROSPECT after model inversion on the VALIDATION dataset (Figure 7). Values
457 obtained with PROSPECT-3 ranged between 2% and 6% over the VIS. This model uses a unique SAC to
458 account for total pigment absorption; therefore it solely applies to healthy green leaves. The
459 dissociation of chlorophylls from carotenoids in PROSPECT-5 explains the strong decrease in RMSE
460 between 400 nm and 500 nm where carotenoids absorb light. However, the discrepancies are still
461 strong between 500 nm and 600 nm where anthocyanins absorb light, and between 650 nm and 750
462 nm, a spectral domain that corresponds to the second absorption peak of chlorophylls. Finally,
463 PROSPECT-D surpassed the previous versions with RMSE ranging between 1% and 2% over the entire
464 VIS.

465

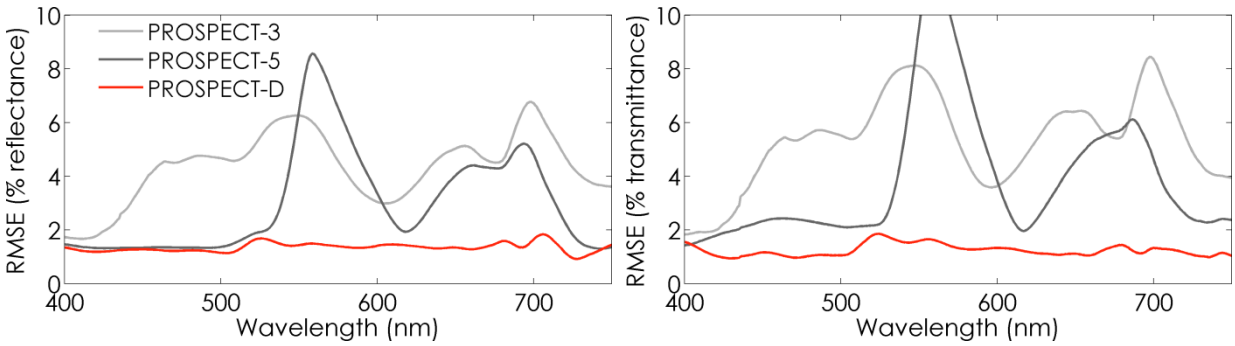

Figure 7. Spectral RMSE between measured and estimated leaf reflectance and transmittance obtained for the VALIDATION dataset after model inversion using PROSPECT-3, PROSPECT-5, and PROSPECT-D.

466

467

468

469 **4.5. Sensitivity to the uncertainty associated with C_{anth} in ANGERS**

470 4.5.a. Specific absorption coefficients

471 The addition of noise to C_{anth} in ANGERS influences the calibration of the SACs of PROSPECT, as
472 expected, but the variability is limited to the 400-500 nm wavelength range, especially for
473 anthocyanins. The main difference for this pigment is observed between 500 nm to 600 nm (Figure
474 8).

475

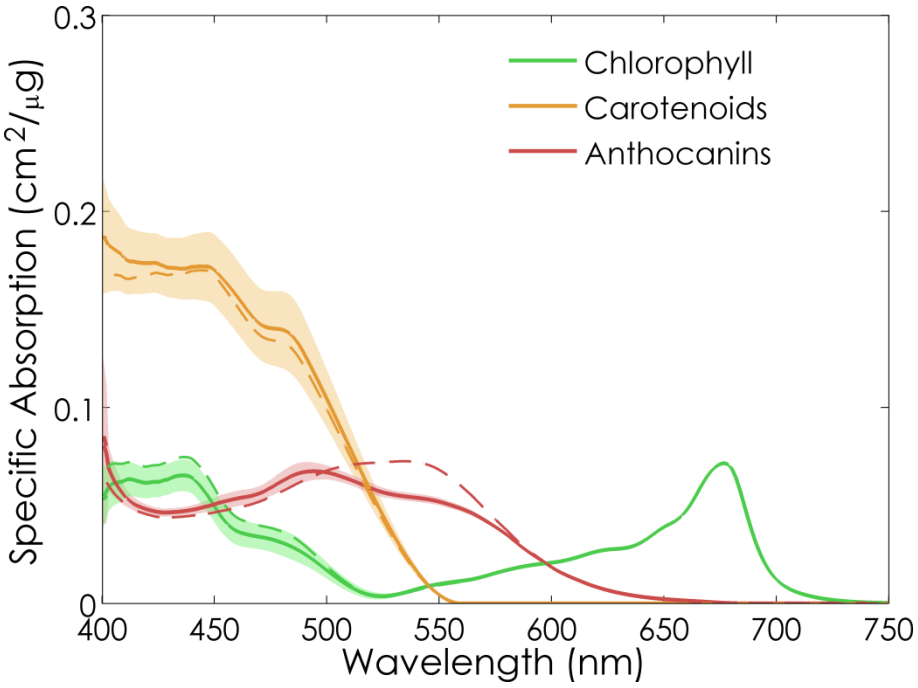

Figure 8. Comparison of the SACs obtained for the three pigments when using C_{anth} values directly derived from $mARI$ (dashed lines) and when using C_{anth} values with noise added corresponding to the error of prediction of C_{anth} observed for experimental data (50 repetitions; plain lines and their envelope correspond to mean value ± 1 standard deviation).

476

477 4.5.b. Estimation of pigment content

478 We estimated pigment content by inverting PROSPECT with the set of SACs derived from noisy C_{anth}.
479 **Erreur ! Source du renvoi introuvable.** summarizes the distributions of RMSE from measured and

480 estimated pigment contents for the validation datasets taken separately and for the VALIDATION
481 dataset that group them together. The uncertainty on C_{anth} has no influence on the estimation of
482 C_{ab}, as the RMSE is close to that obtained when no noise was added to C_{anth}. The influence is higher
483 on the estimation of carotenoids. The version of the model with no noise added to C_{anth}
484 outperformed the versions including noise, particularly for MAPLE. This version also outperformed all
485 noisy versions when focusing on VALIDATION. Finally, the estimation of C_{anth} also performed better
486 when no noise was added to the ANGERS calibration samples, except for MAPLE, which performs a
487 little less now. However as for C_{xc}, the results obtained with VALIDATION showed better estimation
488 of C_{anth} when no noise was added. These results validate the calibration of PROSPECT-D with C_{anth}
489 determined using a spectral index. Moreover, the slight decrease in performances for the estimation
490 of C_{anth} and C_{xc} when adding noise to C_{anth} suggests that the estimated values obtained for C_{anth}
491 in ANGERS may show lower uncertainty than expected based on the experimental data available.

492

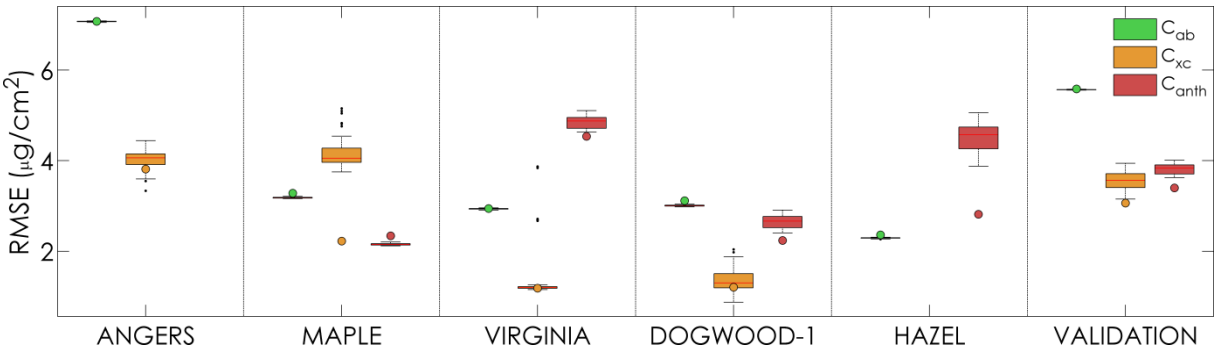

Figure 9. Distribution of the RMSE between measured and estimated pigment content after adding noise to the values of C_{anth} of ANGERS used for calibration of PROSPECT and inversion of the model based on the SACs displayed in Figure 8. Colored dots correspond to the RMSE obtained when no noise is added to C_{anth} in ANGERS.

493

494 4.5.c. Simulation of leaf optical properties

The accuracy of reflectance and transmittance reconstruction is displayed in Figure 10. The spectra simulated by PROSPECT-D show very minor differences whatever noise was added to C_{anth} or not. These results confirm that despite missing values and indirect estimation of C_{anth} for ANGERS, PROSPECT-D provides stable results in terms of calibrated SACs as well as model performance both in direct and inverse modes.

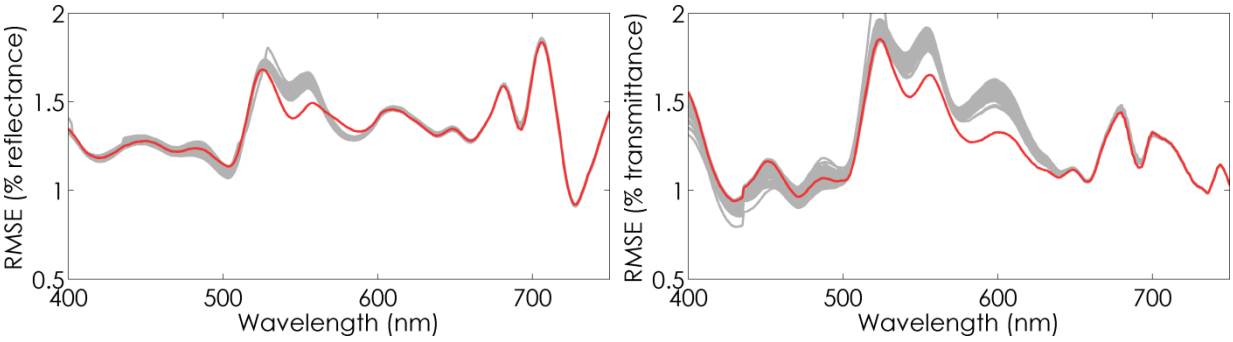

Figure 10. Spectral RMSE between measured and estimated leaf reflectance and transmittance obtained for the VALIDATION dataset after model inversion using PROSPECT-D calibrated with (grey lines) and without (red lines) uncertainty added to C_{anth}.

5. Discussion

5.1. Specific absorption coefficients

As stated earlier, the SAC of anthocyanins obtained after the calibration phase (Figure 5) displayed a broad absorption peak centered on 550 nm. The overall profile agrees well with the spectra obtained in previous studies (Gitelson et al., 2001; Peters and Noble, 2014). We compared this SAC with absorption spectra of pure cyanidin-3-glucoside (C3G), measured in the lab for different pH (Fossen et al., 1998). C3G is also the most common anthocyanin in leaves (Harborne and Williams, 1998). The SACs derived from a model generally do not match data published in the literature for *in vitro* dissolved pigments. Several causes may explain such a discrepancy. First, radiative transfer model are imperfect: for instance, a two-layer model taking into account the

asymmetry of leaf anatomy and chemical content in Dicots may improve the determination of the SACs. Moreover, the calibration of these models is based on experimental data which may be not optimal in terms of sampling, despite our efforts to provide the best experimental datasets. Second, molecules *in vivo* are linked to their environment, which may induce shifts in their SACs: this is the case for chlorophylls with proteins, or anthocyanins with the pH or temperature (Figueiredo et al., 1999; Yabuya et al., 1999; Boulton, 2001). Thirdly, while the model assumes stable compositions and absorption spectra for chlorophylls, carotenoids and anthocyanins, in reality these are families of pigments containing between two and hundreds of molecules, with as many variations in their particular absorption spectra. Subtle changes in anthocyanin composition, chlorophyll *a*:*b* ratio, or induced by the xanthophyll cycle may result in variations in leaf reflectance and transmittance that are detectable but not interpretable by PROSPECT. Finally, as explained earlier, internal multiple scattering (detour effect) and distributional errors (sieve effect) may also explain part of the discrepancies observed between *in vivo* and *in vitro* SACs. **Figure 11**shows the profile of the SAC of anthocyanins: it is intermediate between the absorption coefficient measured for C3G at pH 1 and pH 8.1 in the main absorption domain of this constituent. The increasing absorption closer to the UV-A may be explained by the presence of flavonols in some leaves: these molecules, which are biosynthetically associated with anthocyanins in plant secondary metabolism, are also optically active in this domain. Therefore, it is likely that flavonols contribute to the anthocyanin SAC spectrum (Solovchenko et al., 2001). The improvement of C_{xc} estimation accuracy upon incorporation of anthocyanins into PROSPECT-D may stem from the inherent correlation between anthocyanin and flavonoid content.

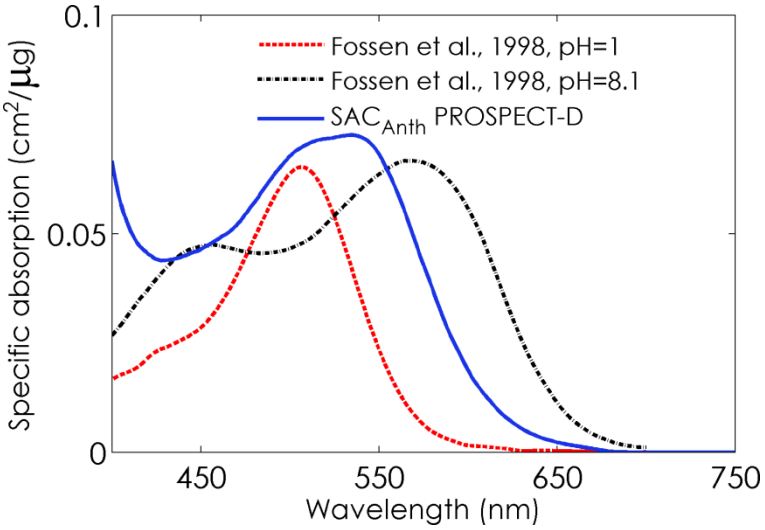

Figure 11. Comparison of the SAC corresponding to anthocyanins derived from PROSPECT-D calibration (cm^2 μg^{-1}) and the absorption of pure Cyanidin 3-glucoside at pH 1 and 8.1 (unitless) (after Fossen et al., 1998).

534

535 The SAC of carotenoids above 450 nm is very similar in PROSPECT-5 and PROSPECT-D. However
536 the estimation of C_{xc} is substantially improved in the latter, which highlights the high sensitivity of
537 PROSPECT to very small changes of the SAC, as well as the importance of incorporating anthocyanins
538 into the model even for leaves with low content. This improvement in the estimation of C_{xc} was not
539 explained by the differences observed between 400 nm and 450nm: when using all the ANGERS
540 dataset for calibration, the SAC calibrated for C_{xc} showed very similar profile as in PROSPECT-5, but
541 the improvement in the estimation of C_{xc} was still observed.

542

543 **5.2. Illustration of the improved simulation of leaf optical properties**

544 To illustrate the ability of PROSPECT-D to simulate leaf optical properties we selected some
545 samples including senescent and reddish leaves (Figure 12). In some cases, the fit is poor: the
546 reflectance spectrum of *Eucalyptus gunnii* is very high compared to that of other leaves, probably
547 due to the presence of wax at the leaf surface, a layer that is not accounted for in PROSPECT (Figure

548 12h). Barry and Newnham (2012) already pointed out an incorrect assessment of carotenoid content
549 in *Eucapyptus globulus* and *Eucapyptus nitens leaves*. The development of PROSPECT-D partly
550 answers these limitations, but further efforts will be needed to include specular reflection (Bousquet
551 et al., 2005; Comar et al., 2014; Jay et al., 2016).
552

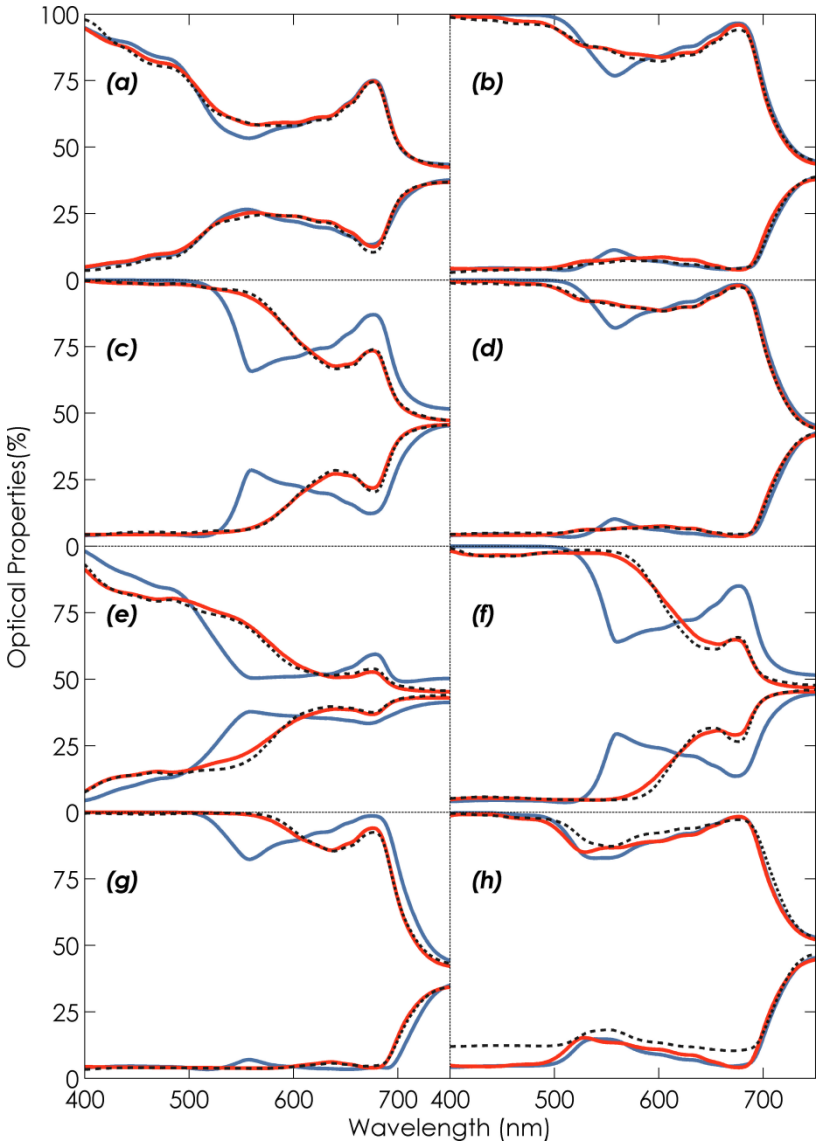

Figure 12. Measured (black dotted line) versus simulated (blue line for PROSPECT-5 and red line for PROSPECT-D) reflectance (lower spectra) and transmittance (upper spectra). (a-b) *Acer pseudoplatanus* L., (c) *Acer platanoides* L., (d) *Corylus avellana* L., (e-f) *Parthenocissus quinquefolia* (L.) Planch., (g) *Corylus maxima 'Purpurea'*, and (h) *Eucalyptus gunnii*. Samples (b-e-f) show non-

senescent anthocyanic leaves, while samples (a-c-d-g) show anthocyanic senescent leaves.

6. Conclusion

We introduced a new, physically-based model called PROSPECT-D which, for the first time, includes the three main families of leaf pigments as independent constituents: chlorophylls, carotenoids, and anthocyanins. PROSPECT-D outperformed the previous versions of the model, both for the estimation of leaf chemical constituents and the simulation of leaf optical properties, on datasets encompassing a broad range of growth conditions and stages. Inversion of PROSPECT-D showed improved estimation of pigment content, especially carotenoid content. These results demonstrate the ability of this new model to simulate optical properties during the lifespan of the leaf and for a new range of conditions, including juvenile and senescent stages, as well as environmental stresses.

We studied the influence of the uncertainty corresponding to the values of C_{anth} from ANGERS used for the calibration of PROSPECT-D. Our results showed that this uncertainty has little to no impact on the calibration, and on the performances of the model in terms of pigment prediction accuracy, as well as in modeling of leaf optics.

The availability of this model has strong implications for vegetation modeling both at leaf and canopy scales. At the leaf scale, PROSPECT-D will allow to perform sensitivity analyses focused on anthocyanins, and to design new vegetation indices dedicated to specific pigments and less sensitive to other ones. The linkage of PROSPECT-D with canopy reflectance models such as SAIL (e.g., Jacquemoud et al., 2009) or DART (Hernández-Clemente et al., 2012; Gastellu-Etchegorry et al., 2015) will allow simulations of vegetation types that could not be reproduced before. Applications for stress and senescence detection will directly take advantage of such improvements. Finally PROSPECT-D is a powerful tool for determining the potential of operational multispectral satellites (Sentinel-2, LandSat-8, WorldView-3) and future hyperspectral missions (EnMAP, Hyspiri, HYPXIM) for fine detection of leaf pigments.

Acknowledgments

The authors warmly thank Luc Bidel, Christophe François and Gabriel Pavan who collected the ANGERS dataset. We also thank Zoran Cerovic (Laboratoire Ecologie-Systématique-Evolution) for the fruitful discussions about leaf pigments. We thank Alexei Solovchenko for his careful review and valuable comments during the preparation of this manuscript. We thank the two anonymous reviewers for their constructive comments and suggestions. Jean-Baptiste Féret was funded by the HyperTropik project (TOSCA program grant of the French Space Agency, CNES), and by Hypos project (European Space Agency, ESA). Jean-Baptiste Féret and Stéphane Jacquemoud were funded by the CHLORμS project (TOSCA program grant of the French Space Agency, CNES). Anatoly Gitelson was supported by Marie Curie International Incoming Visiting Professor Fellowship. Scott Noble was supported by the Natural Sciences and Engineering Research Council (NSERC) Discovery Grant program and University of Saskatchewan sabbatical travel fund.

References

Allen, W.A., Gausman, H.W., Richardson, A.J., 1970. Mean effective optical constants of cotton leaves. J. Opt. Soc. Am. 60, 542–547. doi:10.1364/JOSA.60.000542

Allen, W.A., Gausman, H.W., Richardson, A.J., Thomas, J.R., 1969. Interaction of isotropic light with a compact plant leaf. J. Opt. Soc. Am. 59, 1376–1379. doi:10.1364/JOSA.59.001376

Asner, G.P., Anderson, C.B., Martin, R.E., Tupayachi, R., Knapp, D.E., Sinca, F., 2015a. Landscape biogeochemistry reflected in shifting distributions of chemical traits in the Amazon forest canopy. Nat. Geosci. 8, 567–573. doi:10.1038/ngeo2443

Asner, G.P., Martin, R.E., 2009. Airborne spectranomics: Mapping canopy chemical and taxonomic diversity in tropical forests. Front. Ecol. Environ. 7, 269–276. doi:10.1890/070152

Asner, G.P., Martin, R.E., Anderson, C.B., Knapp, D.E., 2015b. Quantifying forest canopy traits: Imaging spectroscopy versus field survey. Remote Sens. Environ. 158, 15–27. doi:10.1016/j.rse.2014.11.011

Atzberger, C., Guérif, M., Baret, F., Werner, W., 2010. Comparative analysis of three chemometric techniques for the spectroradiometric assessment of canopy chlorophyll content in winter wheat. Comput. Electron. Agric. 73, 165–173. doi:10.1016/j.compag.2010.05.006

Barry, K., Newnham, G., 2012. Quantification of chlorophyll and carotenoid pigments in eucalyptus foliage with the radiative transfer model PROSPECT 5 is affected by anthocyanin and epicuticular waxes., in: Proc. Geospatial Science Research 2 Symposium, GSR 2012, Melbourne, Australia, December 10-12, 2012.

Blackburn, G.A., 2007. Hyperspectral remote sensing of plant pigments. J. Exp. Bot. 58, 855–867. doi:10.1093/jxb/erl123

614 Boulton, R., 2001. The copigmentation of anthocyanins and its role in the color of red wine: A critical
615 review. Am. J. Enol. Vitic. 52, 67–87.
616 Bousquet, L., Lachérade, S., Jacquemoud, S., Moya, I., 2005. Leaf BRDF measurements and model for
617 specular and diffuse components differentiation. Remote Sens. Environ. 98, 201–211.
618 doi:10.1016/j.rse.2005.07.005
619 Britton, G., Liaaen-Jensen, S., Pfander, H. (Eds.), 2004. Carotenoids. Birkhäuser Basel, Basel.
620 Brockington, S.F., Walker, R.H., Glover, B.J., Soltis, P.S., Soltis, D.E., 2011. Complex pigment evolution
621 in the Caryophyllales: Research review. New Phytol. 190, 854–864. doi:10.1111/j.1469-
622 8137.2011.03687.x
623 Chappelle, E.W., Kim, M.S., McMurtrey, J.E., 1992. Ratio analysis of reflectance spectra (RARS): An
624 algorithm for the remote estimation of the concentrations of chlorophyll A, chlorophyll B,
625 and carotenoids in soybean leaves. Remote Sens. Environ. 39, 239–247. doi:10.1016/0034-
626 4257(92)90089-3
627 Chen, M., Weng, F., 2012. Kramers-Kronig analysis of leaf refractive index with the PROSPECT leaf
628 optical property model: K-K analysis of leaf refractive index. J. Geophys. Res. Atmospheres
629 117, D18106n. doi:10.1029/2012JD017477
630 Comar, A., Baret, F., Obein, G., Simonot, L., Meneveaux, D., Viénot, F., de Solan, B., 2014. ACT: A leaf
631 BRDF model taking into account the azimuthal anisotropy of monocotyledonous leaf surface.
632 Remote Sens. Environ. 143, 112–121. doi:10.1016/j.rse.2013.12.006
633 Davies, K., 2004. Plant pigments and their manipulation. Blackwell ; CRC, Oxford; Boca Raton.
634 Di Vittorio, A.V., 2009. Enhancing a leaf radiative transfer model to estimate concentrations and in
635 vivo specific absorption coefficients of total carotenoids and chlorophylls a and b from single-
636 needle reflectance and transmittance. Remote Sens. Environ. 113, 1948–1966.
637 doi:10.1016/j.rse.2009.05.002
638 Dougall, D.K., Baker, D.C., 2008. Effects of reaction mixture and other components on the
639 determination of the equilibrium and rate constants of the hydration reactions of
640 anthocyanins. Food Chem. 107, 473–482. doi:10.1016/j.foodchem.2007.07.035
641 Féret, J.-B., François, C., Asner, G.P., Gitelson, A.A., Martin, R.E., Bidel, L.P.R., Ustin, S.L., le Maire, G.,
642 Jacquemoud, S., 2008. PROSPECT-4 and 5: Advances in the leaf optical properties model
643 separating photosynthetic pigments. Remote Sens. Environ. 112, 3030–3043.
644 doi:10.1016/j.rse.2008.02.012
645 Féret, J.-B., François, C., Gitelson, A., Asner, G.P., Barry, K.M., Panigada, C., Richardson, A.D.,
646 Jacquemoud, S., 2011. Optimizing spectral indices and chemometric analysis of leaf chemical
647 properties using radiative transfer modeling. Remote Sens. Environ. 115, 2742–2750.
648 doi:10.1016/j.rse.2011.06.016
649 Figueiredo, P., George, F., Tatsuzawa, F., Toki, K., Saito, N., Brouillard, R., 1999. New features of
650 intramolecular copigmentation byacylated anthocyanins. Phytochemistry 51, 125–132.
651 doi:10.1016/S0031-9422(98)00685-2
652 Filella, I., Porcar-Castell, A., Munné-Bosch, S., Bäck, J., Garbulsky, M.F., Peñuelas, J., 2009. PRI
653 assessment of long-term changes in carotenoids/chlorophyll ratio and short-term changes in
654 de-epoxidation state of the xanthophyll cycle. Int. J. Remote Sens. 30, 4443–4455.
655 doi:10.1080/01431160802575661
656 Fossen, T., Cabrita, L., Andersen, O.M., 1998. Colour and stability of pure anthocyanins influenced by
657 pH including the alkaline region. Food Chem. 63, 435–440. doi:10.1016/S0308-
658 8146(98)00065-X
659 Fukshansky, L., Remisowsky, A.M.V., McClendon, J., Ritterbusch, A., Richter, T., Mohr, H., 1993.
660 Absorption spectra of leaves corrected for scattering and distributional error: a radiative
661 transfer and absorption statistics treatment. Photochem. Photobiol. 57, 538–555.
662 doi:10.1111/j.1751-1097.1993.tb02332.x
663 Gamon, J.A., Field, C.B., Bilger, W., Björkman, O., Fredeen, A.L., Peñuelas, J., 1990. Remote sensing of
664 the xanthophyll cycle and chlorophyll fluorescence in sunflower leaves and canopies.
665 Oecologia 85, 1–7. doi:10.1007/BF00317336

666 Gamon, J.A., Huemmrich, K.F., Wong, C.Y.S., Ensminger, I., Garrity, S., Hollinger, D.Y., Noormets, A.,
667 Peñuelas, J., 2016. A remotely sensed pigment index reveals photosynthetic phenology in
668 evergreen conifers. Proc. Natl. Acad. Sci. 113, 13087–13092. doi:10.1073/pnas.1606162113
669 Gamon, J.A., Peñuelas, J., Field, C.B., 1992. A narrow-waveband spectral index that tracks diurnal
670 changes in photosynthetic efficiency. Remote Sens. Environ. 41, 35–44. doi:10.1016/0034-
671 4257(92)90059-S
672 Gamon, J.A., Serrano, L., Surfus, J.S., 1997. The photochemical reflectance index: an optical indicator
673 of photosynthetic radiation use efficiency across species, functional types, and nutrient
674 levels. Oecologia 112, 492–501. doi:10.1007/s004420050337
675 Gamon, J.A., Surfus, J.S., 1999. Assessing leaf pigment content a nd activity with a reflectometer.
676 New Phytol. 105–117.
677 Gastellu-Etchegorry, J.-P., Yin, T., Lauret, N., Cajgfinger, T., Gregoire, T., Grau, E., Féret, J.-B., Lopes,
678 M., Guilleux, J., Dedieu, G., Malenovský, Z., Cook, B., Morton, D., Rubio, J., Durrieu, S.,
679 Cazanave, G., Martin, E., Ristorcelli, T., 2015. Discrete anisotropic radiative transfer (DART 5)
680 for modeling airborne and satellite spectroradiometer and LIDAR acquisitions of natural and
681 urban landscapes. Remote Sens. 7, 1667–1701. doi:10.3390/rs70201667
682 Gitelson, A.A., 2005. Remote estimation of canopy chlorophyll content in crops. Geophys. Res. Lett.
683 32. doi:10.1029/2005GL022688
684 Gitelson, A.A., Chivkunova, O.B., Merzlyak, M.N., 2009. Nondestructive estimation of anthocyanins
685 and chlorophylls in anthocyanic leaves. Am. J. Bot. 96, 1861–1868. doi:10.3732/ajb.0800395
686 Gitelson, A.A., Keydan, G.P., Merzlyak, M.N., 2006. Three-band model for noninvasive estimation of
687 chlorophyll, carotenoids, and anthocyanin contents in higher plant leaves. Geophys. Res.
688 Lett. 33, L11402. doi:10.1029/2006GL026457
689 Gitelson, A.A., Merzlyak, M.N., Chivkunova, O.B., 2001. Optical properties and nondestructive
690 estimation of anthocyanin content in plant leaves. Photochem. Photobiol. 74, 38–45.
691 doi:10.1562/0031-8655(2001)074<0038:OPANEO>2.0.CO;2
692 Gitelson, A.A., Peng, Y., Masek, J.G., Rundquist, D.C., Verma, S., Suyker, A., Baker, J.M., Hatfield, J.L.,
693 Meyers, T., 2012. Remote estimation of crop gross primary production with Landsat data.
694 Remote Sens. Environ. 121, 404–414. doi:10.1016/j.rse.2012.02.017
695 Gould, K., Davies, K., Winefield, C. (Eds.), 2009. Anthocyanins: Biosynthesis, functions, and
696 applications. Springer, New York, NY.
697 Gould, K.S., 2004. Nature's swiss army knife: The diverse protective roles of anthocyanins in leaves. J.
698 Biomed. Biotechnol. 2004, 314–320. doi:10.1155/S1110724304406147
699 Haboudane, D., 2004. Hyperspectral vegetation indices and novel algorithms for predicting green LAI
700 of crop canopies: Modeling and validation in the context of precision agriculture. Remote
701 Sens. Environ. 90, 337–352. doi:10.1016/j.rse.2003.12.013
702 Hale, G.M., Querry, M.R., 1973. Optical constants of water in the 200-nm to 200-µm wavelength
703 region. Appl. Opt. 12, 555–562. doi:10.1364/AO.12.000555
704 Harborne, J.B., Williams, C.A., 1998. Anthocyanins and other flavonoids. Nat. Prod. Rep. 15, 631–652.
705 doi:10.1039/a815631y
706 Hernández-Clemente, R., Navarro-Cerrillo, R.M., Zarco-Tejada, P.J., 2014. Deriving predictive
707 relationships of carotenoid content at the canopy level in a conifer forest using hyperspectral
708 imagery and model simulation. IEEE Trans. Geosci. Remote Sens. 52, 5206–5217.
709 doi:10.1109/TGRS.2013.2287304
710 Hernández-Clemente, R., Navarro-Cerrillo, R.M., Zarco-Tejada, P.J., 2012. Carotenoid content
711 estimation in a heterogeneous conifer forest using narrow-band indices and PROSPECT+
712 DART simulations. Remote Sens. Environ. 127, 298–315. doi:doi:10.1016/j.rse.2012.09.014
713 Hmimina, G., Merlier, E., DufrêNe, E., Soudani, K., 2015. Deconvolution of pigment and
714 physiologically related photochemical reflectance index variability at the canopy scale over
715 an entire growing season: Towards an understanding of canopy PRI variability. Plant Cell
716 Environ. 38, 1578–1590. doi:10.1111/pce.12509

Jacquemoud, S., Baret, F., 1990. PROSPECT: A model of leaf optical properties spectra. Remote Sens. Environ. 34, 75–91. doi:10.1016/0034-4257(90)90100-Z

Jacquemoud, S., Verhoef, W., Baret, F., Bacour, C., Zarco-Tejada, P.J., Asner, G.P., François, C., Ustin, S.L., 2009. PROSPECT+ SAIL models: A review of use for vegetation characterization. Remote Sens. Environ. 113, S56–S66. doi:doi:10.1016/j.rse.2008.01.026

Jay, S., Bendoula, R., Hadoux, X., Féret, J.-B., Gorretta, N., 2016. A physically-based model for retrieving foliar biochemistry and leaf orientation using close-range imaging spectroscopy. Remote Sens. Environ. 177, 220–236. doi:10.1016/j.rse.2016.02.029

Joiner, J., Yoshida, Y., Vasilkov, A.P., Yoshida, Y., Corp, L.A., Middleton, E.M., 2011. First observations of global and seasonal terrestrial chlorophyll fluorescence from space. Biogeosciences 8, 637–651. doi:10.5194/bg-8-637-2011

le Maire, G., François, C., Dufrêne, E., 2004. Towards universal broad leaf chlorophyll indices using PROSPECT simulated database and hyperspectral reflectance measurements. Remote Sens. Environ. 89, 1–28. doi:10.1016/j.rse.2003.09.004

Lee, D., Gould, K., 2002. Why Leaves Turn Red: : Pigments called anthocyanins probably protect leaves from light damage by direct shielding and by scavenging free radicals,. Am. Sci. 90, 524–528. doi:10.1511/2002.6.524

Lev-Yadun, S., Gould, K.S., 2008. Role of anthocyanins in plant defence, in: Winefield, C., Davies, K., Gould, K. (Eds.), Anthocyanins. Springer New York, New York, NY, pp. 22–28.

Li, P., Wang, Q., 2011. Retrieval of leaf biochemical parameters using PROSPECT inversion: A new approach for alleviating ill-posed problems. IEEE Trans. Geosci. Remote Sens. 49, 2499–2506. doi:10.1109/TGRS.2011.2109390

Lucarini, V., Saarinen, J.J., Peiponen, K.-E., Vartiainen, E.M. (Eds.), 2005. Kramers-Kronig relations in optical materials research, Springer series in optical sciences. Springer, Berlin.

Maier, S.W., Lüdeker, W., Günther, K.P., 1999. SLOP: : a revised version of the stochastic model for leaf optical properties. Remote Sens. Environ. 68, 273–280. doi:10.1016/S0034-4257(98)00118-7

Malenovský, Z., Albrechtová, J., Lhotáková, Z., Zurita-Milla, R., Clevers, J.G.P.W., Schaepman, M.E., Cudlín, P., 2006. Applicability of the PROSPECT model for Norway spruce needles. Int. J. Remote Sens. 27, 5315–5340. doi:10.1080/01431160600762990

Marquart, L.C., 1835. Die Farben der Blüthen: Eine Chemisch-Physiologische Abhandlung. Verlag von T. Habicht, Bonn.

Martinière, A., Bassil, E., Jublanc, E., Alcon, C., Reguera, M., Sentenac, H., Blumwald, E., Paris, N., 2013. In vivo intracellular pH measurements in tobacco and arabidopsis reveal an unexpected pH gradient in the endomembrane system. Plant Cell 25, 4028–4043. doi:10.1105/tpc.113.116897

Mathieu, Y., Guern, J., Kurkdjian, A., Manigault, P., Manigault, J., Zielinska, T., Gillet, B., Beloeil, J.-C., Lallemand, J.-Y., 1989. Regulation of vacuolar pH of plant cells: I. isolation and properties of vacuoles suitable for ^{31}P NMR studies. Plant Physiol. 89, 19–26. doi:10.1104/pp.89.1.19

Matile, P., 2000. Biochemistry of Indian summer: physiology of autumnal leaf coloration. Exp. Gerontol. 35, 145–158. doi:10.1016/S0531-5565(00)00081-4

Merzlyak, M.N., Chivkunova, O.B., Solovchenko, A.E., Naqvi, K.R., 2008. Light absorption by anthocyanins in juvenile, stressed, and senescing leaves. J. Exp. Bot. 59, 3903–3911. doi:10.1093/jxb/ern230

Nakaji, T., Oguma, H., Fujinuma, Y., 2006. Seasonal changes in the relationship between photochemical reflectance index and photosynthetic light use efficiency of Japanese larch needles. Int. J. Remote Sens. 27, 493–509. doi:10.1080/01431160500329528

Peng, Y., Gitelson, A.A., 2012. Remote estimation of gross primary productivity in soybean and maize based on total crop chlorophyll content. Remote Sens. Environ. 117, 440–448. doi:10.1016/j.rse.2011.10.021

Peters, R.D., Noble, S.D., 2014. Spectrographic measurement of plant pigments from 300 to 800nm. Remote Sens. Environ. 148, 119–123. doi:10.1016/j.rse.2014.03.020

769 Pfündel, E.E., Ben Ghozlen, N., Meyer, S., Cerovic, Z.G., 2007. Investigating UV screening in leaves by
770 two different types of portable UV fluorimeters reveals in vivo screening by anthocyanins
771 and carotenoids. Photosynth. Res. 93, 205–221. doi:10.1007/s11120-007-9135-7
772 Richardson, A.D., Duigan, S.P., Berlyn, G.P., 2002. An evaluation of noninvasive methods to estimate
773 foliar chlorophyll content. New Phytol. 153, 185–194. doi:10.1046/j.0028-646X.2001.00289.x
774 Rühle, W., Wild, A., 1979. The intensification of absorbance changes in leaves by light-dispersion:
775 Differences between high-light and low-light leaves. Planta 146, 551–557.
776 doi:10.1007/BF00388831
777 Rundquist, D., Gitelson, A., Leavitt, B., Zygielbaum, A., Perk, R., Keydan, G., 2014. Elements of an
778 integrated phenotyping system for monitoring crop status at canopy level. Agronomy 4, 108–
779 123. doi:10.3390/agronomy4010108
780 Shipley, B., Lechowicz, M.J., Wright, I., Reich, P.B., 2006. Fundamental trade-offs generating the
781 worldwide leaf economics spectrum. Ecology 87, 535–541. doi:10.1890/05-1051
782 Sims, D.A., Gamon, J.A., 2002. Relationships between leaf pigment content and spectral reflectance
783 across a wide range of species, leaf structures and developmental stages. Remote Sens.
784 Environ. 81, 337–354. doi:10.1016/S0034-4257(02)00010-X
785 Solovchenko, A.E., Chivkunova, O.B., Merzlyak, M.N., Reshetnikova, I.V., 2001. A spectrophotometric
786 analysis of pigments in apples. Russ. J. Plant Physiol. 48, 693–700.
787 doi:10.1023/A:1016780624280
788 Steele, M.R., Gitelson, A.A., Rundquist, D.C., Merzlyak, M.N., 2009. Nondestructive estimation of
789 anthocyanin content in grapevine leaves. Am. J. Enol. Vitic. 60, 87–92.
790 Stuckens, J., Verstraeten, W.W., Delalieux, S., Swennen, R., Coppin, P., 2009. A dorsiventral leaf
791 radiative transfer model: Development, validation and improved model inversion techniques.
792 Remote Sens. Environ. 113, 2560–2573. doi:10.1016/j.rse.2009.07.014
793 Stylinski, C., Gamon, J., Oechel, W., 2002. Seasonal patterns of reflectance indices, carotenoid
794 pigments and photosynthesis of evergreen chaparral species. Oecologia 131, 366–374.
795 doi:10.1007/s00442-002-0905-9
796 Ustin, S.L., Gitelson, A.A., Jacquemoud, S., Schaepman, M., Asner, G.P., Gamon, J.A., Zarco-Tejada, P.,
797 2009. Retrieval of foliar information about plant pigment systems from high resolution
798 spectroscopy. Remote Sens. Environ. 113, S67–S77. doi:10.1016/j.rse.2008.10.019
799 van den Berg, A.K., Perkins, T.D., 2005. Nondestructive estimation of anthocyanin content in autumn
800 sugar maple leaves. HortScience 40, 685–686.
801 Verhoef, W., 1984. Light scattering by leaf layers with application to canopy reflectance modeling:
802 The SAIL model. Remote Sens. Environ. 16, 125–141. doi:10.1016/0034-4257(84)90057-9
803 Verhoef, W., Jia, L., Xiao, Q., Su, Z., 2007. Unified optical-thermal four-stream radiative transfer
804 theory for homogeneous vegetation canopies. IEEE Trans. Geosci. Remote Sens. 45, 1808–
805 1822. doi:10.1109/TGRS.2007.895844
806 Verrelst, J., Camps-Valls, G., Muñoz-Marí, J., Rivera, J.P., Veroustraete, F., Clevers, J.G.P.W., Moreno,
807 J., 2015. Optical remote sensing and the retrieval of terrestrial vegetation bio-geophysical
808 properties – A review. ISPRS J. Photogramm. Remote Sens. 108, 273–290.
809 doi:10.1016/j.isprsjprs.2015.05.005
810 Yabuya, T., Nakamura, M., Iwashina, T., Yamaguchi, M., Takehara, T., 1997. Anthocyanin-flavone
811 copigmentation in bluish purple flowers of Japanese garden iris (*Iris ensata* Thunb.).
812 Euphytica 98, 163–167. doi:10.1023/A:1003152813333
813 Zarco-Tejada, P.J., Guillén-Climent, M.L., Hernández-Clemente, R., Catalina, A., González, M.R.,
814 Martín, P., 2013. Estimating leaf carotenoid content in vineyards using high resolution
815 hyperspectral imagery acquired from an unmanned aerial vehicle (UAV). Agric. For.
816 Meteorol. 171–172, 281–294. doi:10.1016/j.agrformet.2012.12.013
817

818 **Figure 1.** Relationship between C_{anth} obtained from wet chemistry and C_{anth} estimated from
819 reflectance data after application of Eq. 2. The black dots correspond to the 137 leaf samples with
820 $mARI < 5$ (R^2 = 0.90) and the grey dots correspond to the 76 leaf samples with $mARI > 5$ (R^2 =
821 0.37). Eq. 2 was adjusted only on the black dots.
822
823 **Figure 2.** Comparison of the refractive index used in PROSPECT-3 (red dots), PROSPECT-5 (grey
824 diamonds) and corresponding to the mean refractive index proposed by (Chen and Weng, 2012)
825 (blue squares). The grey area corresponds to the range of variation of the refractive index proposed
826 by Chen and Weng, (2012); the plain grey line corresponds to the refractive index for pure liquid
827 water (Hale and Querry, 1973).
828
829 **Figure 3.** Stacked distribution of pigment content for the calibration and validation samples selected
830 from ANGERS and VIRGINIA. Light colors: calibration (144 samples from ANGERS, 20 Samples from
831 VIRGINIA); dark colors: validation (164 samples from ANGERS, 61 samples from VIRGINIA).
832
833 **Figure 4.** Spectral RMSE between measured leaf optics and simulated reflectance (left), and
834 transmittance (right) obtained after model inversion with the refractive index used in PROSPECT-5
835 (black dotted line), PROSPECT-3 (red), and derived from Chen and Weng (2012) (light grey).
836
837 **Figure 5.** Specific absorption coefficients of chlorophylls (green), carotenoids (orange), and
838 anthocyanins (red). The solids line correspond to the SAC of all the pigments in PROSPECT-D, the
839 dashed lines to the SAC of chlorophylls and carotenoids in PROSPECT-5, and to the SAC of
840 anthocyanins measured by Peters and Noble (2014) using thin layer chromatography.
841

842 **Figure 6.** Estimation of pigment content by inversion of three versions of PROSPECT on six datasets
843 (when relevant). Red dots correspond to calibration samples from ANGERS and VIRGINIA.
844
845 **Figure 7.** Spectral RMSE between measured and estimated leaf reflectance and transmittance
846 obtained for the VALIDATION dataset after model inversion using PROSPECT-3, PROSPECT-5, and
847 PROSPECT-D.
848
849 **Figure 8.** Comparison of the SACs obtained for the three pigments when using C_{anth} values directly
850 derived from $mARI$ (dashed lines) and when using C_{anth} values with noise added corresponding to
851 the error of prediction of C_{anth} observed for experimental data (50 repetitions; plain lines and their
852 envelope correspond to mean value ± 1 standard deviation).
853
854 **Figure 9.** Distribution of the RMSE between measured and estimated pigment content after adding
855 noise to the values of C_{anth} of ANGERS used for calibration of PROSPECT and inversion of the model
856 based on the SACs displayed in Figure 8. Colored dots correspond to the RMSE obtained when no
857 noise is added to C_{anth} in ANGERS.
858
859 **Figure 10.** Spectral RMSE between measured and estimated leaf reflectance and transmittance
860 obtained for the VALIDATION dataset after model inversion using PROSPECT-D calibrated with (grey
861 lines) and without (red lines) uncertainty added to C_{anth}.
862
863 **Figure 11.** Comparison of the SAC corresponding to anthocyanins derived from PROSPECT-D
864 calibration (cm^2 μg^{-1}) and the absorption of pure Cyanidin 3-glucoside at pH 1 and 8.1 (unitless) (after
865 Fossen et al., 1998).
866

867 **Figure 12.** Measured (black dotted line) versus simulated (blue line for PROSPECT-5 and red line for
868 PROSPECT-D) reflectance (lower spectra) and transmittance (upper spectra). (a-b) *Acer*
869 *pseudoplatanus* L., (c) *Acer platanoides* L., (d) *Corylus avellana* L., (e-f) *Parthenocissus quinquefolia*
870 (L.) Planch., (g) *Corylus maxima 'Purpurea'*, and (h) *Eucalyptus gunnii*. Samples (b-e-f) show non-
871 senescent anthocyanic leaves, while samples (a-c-d-g) show anthocyanic senescent leaves.
872
873 **Table 1.** Description of the leaf datasets used in this study.
874
875 **Table 2.** RMSE (µg cm^{-2}) of the estimation of leaf pigment content using PROSPECT-3 (P-3),
876 PROSPECT-5 (P-5), and PROSPECT-D (P-D) inversion. The bold font for numbers indicates the lowest
877 values.
878